Mutual manipulation between a dark soliton and a probe wave for the gray-dark solitonic well

Jifang Rong [1], Hua Yang,[1,2,*] Yuzhe Xiao,[3] and Yufang Chen[1]

[1]*College of Computer Science and Electronic Engineering, Key Laboratory for Micro/Nano Optoelectronic Devices of Ministry of Education, Hunan University, Changsha 410082, China*
[2]*Synergetic Innovation Center for Quantum Effects and Application, Hunan Normal University, Changsha 410082, China*
[3]*Department of Electrical Engineering, University of Wisconsin-Madison, Madison, Wisconsin 53715, USA*

We propose an approach to actively control the formation of the dark solitonic well by adjusting the input properties of both the dark solitons and probe waves under the fiber-optical analog of the event horizon. An interesting process of the trapping of a probe wave by the gray solitonic well is demonstrated here, which is accompanied by a transformation between the gray and black solitonic wells. This solitonic well transformation and control process originates from the intrinsic competition between the probe-soliton collision-induced nonlinear phase shift and the internal phase of the dark soliton. The trapping efficiency is sensitive to both the grayness value of the input dark soliton and the frequency of the launched probe wave. The solitonic well investigated as a combination of white- and black-hole horizon can be considered as a qualified candidate for achieving the photonic transistorlike action. The study of a gray-black solitonic well proves the theory basis for further understanding of the light-by-light controlling in a more controllable manner.

I. INTRODUCTION

The light-by-light controlling as a research hotspot has been widely used in high-efficient pulse compression [1,2], optical rogue wave formation [3–5], as well as all-optical transistors [6,7]. During these dynamics, the intense soliton prevents the penetration of the weak probe wave with slightly different transmission velocities, giving rise to an artificial event horizon [7–9]. To the probe wave, the soliton boundary appears as the analog of the white- and black-hole horizon at the trailing and the leading edge of the energetic soliton, respectively, where the probe wave can neither enter nor escape [6,10,11]. The underlying physical mechanism for the interaction between the two pulses was termed as the soliton-induced Kerr effect, where the intensity-dependent refractive index leads to the temporal reflection on the edge of the energetic soliton, which further changes the group velocity of the probe wave [12–14]. The transmission velocity change of the probe wave is directly due to the nonlinear optical frequency conversion between the probe wave and the reflected wave, resulting in the blue- and red-shift at the white- and black-hole horizon, respectively [15–18]. The frequency conversion process is reversible when the probe wave is relatively weak and cannot scatter the soliton in the regime of the optical event horizon [19]. A vital feature during the collision dynamics is that the collision affects not only the transmission properties of the probe wave but also the dynamic of the soliton [15–19]. Previous studies have shown that the underlying physical principle for generating new frequency components can be a productive way to generate ultrabroadband and coherent supercontinuum without either soliton fissionor modulation instability [20,21]. Moreover, it has been shown that the solitonic well consisting of two intense solitons can trap a weak probe wave, via both numerical simulations [13,16,22] and experimental demonstration [23]. However, investigations on the collision dynamics and the solitonic well at the optical event horizon are primarily focused on the active control of fundamental [7–11,19–21] and higher-order bright solitons [16,24], and only a few studies focused on dark solitons [25–28].

The dark solitons only existing in the normal dispersion regime appear as localized notches over a continuous wave background with uniform intensity and are modulationally stable [29]. Research interest in dark solitons was motivated by the observations of temporal dark solitons in several experiments in optical systems several decades ago [30,31]. Since then the physical mechanisms underlying dark solitons propagation have attracted extensive interest and have been applied to nonlinear problems with different contexts, especially in the field of nonlinear optics. The dark solitons perturbed by both high-order dispersion (HOD) and nonlinear effects also have been investigated theoretically [29,32,33] and experimentally [34,35]. It was demonstrated in these studies that the wavelength and intensity of the emitted DWs can be adjusted by the soliton grayness, the intensity of HOD, as well as the Rama effect. In addition, C. Milián *et al.* have proposed the possibility to form a continuum with the dispersion waves (DWs) emitted by dark soliton trains for the first time in 2009 [33]. Recently, it has been found that two intense black solitons can form a solitonic well where DWs can be trapped [18]. The transformation between gray and black solitons has also been discovered by adjusting the probe wave parameters through the nonlinear interaction [36]. All this shows that the nonlinear interaction between the dark

*huayang@hnu.edu.cn

023505-1

soliton and the probe wave is still an attractive research field. However, to the best of our knowledge, the basic mechanism for the transformation process has not been systematically investigated at the fiber-optical analog of an event horizon, which is considered to be the cornerstone of the manipulation of the collision dynamics, the formation of a gray solitonic well, as well as the transformation of black and gray solitonic wells.

In this article, we numerically demonstrate mutual manipulation between a dark soliton in the normal dispersion regime and a DW in the abnormal dispersion regime at the optical event horizon, which provides a novel view on the manipulation of the collision dynamics to control the formation of an effective solitonic well. Adjusting the time delay and the intensity of the probe wave according to the soliton grayness achieves the soliton manipulation and ultimately realizes the flexible variation of soliton grayness, including the transformation between black and gray solitons. In addition, it is shown that the reflected wave energy conversion efficiency and the output spectrum of the probe wave after the collision can be largely regulated by controlling both the input soliton grayness and the frequency of the incident probe wave. Finally, we realize the DW trapping by a gray solitonic well and the transformation between gray and black solitonic wells.

II. THEORETICAL MODEL

The typical collision process between the dark soliton and the probe wave at the fiber-optical analog of the event horizon in the dispersive nonlinear optical fiber can be governed by the following normalized nonlinear Schrödinger equation [37,38]:

$$i\partial_z A - \frac{1}{2}\partial_t^2 A + i\varepsilon\partial_t^3 A + |A|^2 A = 0. \quad (1)$$

Here, A is the normalized electric envelope, z is the normalized transmission distance along with the fiber, and t is dimensionless time, and they satisfy the following relations: $z = Z/Z_0$, $t = [T - Z/\upsilon(\omega_0)]/T_0$. Among them, $Z_0 = T_0^2/|\beta_2|$, ω_0 is the center carrier frequency of the dark soliton, and $\upsilon(\omega_0)$ is the corresponding group velocity. The coefficient $\varepsilon = \beta_3/(6|\beta_2|T_0)$ denotes the relative intensity of third-order dispersion. Particularly, $\varepsilon \neq 0$ is the fundamental condition for the formation of the fiber-optical analog of the event horizon. We ignore HOD ($n > 3$), Raman effect, and self-steepening to focus only on the main physical factors during light-by-light controlling. Indeed, this assumption is reasonable because the Raman effect, self-steepening effect, as well as the HOD with $n > 3$ can be neglected in the regime of propagation dynamics at the optical event horizon [7,16,39]. The input field $A(0, t)$ consists of two pulses—the dark soliton and the probe wave—that do not overlap both temporally and spectrally:

$$A(0, t) = A_{\mathrm{ds}}(0, t) + A_p(0, t). \quad (2)$$

Here, $A_p(0, t)$ is a hyperbolic secant pulse with a delay t_1 and a frequency offset of f.

$$A_p(0, t) = A_p\mathrm{sech}[(t + t_1)/T_1]\exp(-i2\pi f). \quad (3)$$

A_p and T_1 are the amplitude and the width of the probe wave. If we consider $\varepsilon = 0$, a dark soliton solution $A_{\mathrm{ds}}(0, t)$ deduced

from Eq. (1) has the following form [29]:

$$A_{\mathrm{ds}}(0, t) = u_0[\cos\phi \tanh(u_0 t \cos\phi) - i\sin\phi], \quad (4)$$

where u_0 is the background amplitude of the dark soliton. Here we pick $u_0 = 1$, for simplicity. The effective angle (phase) $\phi(|\phi| \leqslant \pi/2)$ corresponds to the total phase shift (2ϕ) across the dark soliton, which is connected with the grayness value ($\cos\phi$) as well as the velocity ($\sin\phi$) of the dark soliton. The soliton with $\phi = 0$ is defined as a black soliton; otherwise, a gray one. The black soliton has an abrupt π phase jump in the center with an intensity value of zero, while the gray solitons have a smaller and smoother phase jump, as well as a nonzero intensity at the pulse center. Furthermore, dark solitons with $\phi > 0$ or $\phi < 0$ travel with a group velocity slower or faster than that at the central carrier frequency ($\phi = 0$), respectively [26].

In the presence of HOD ($n \geqslant 3$), dark solitons emit phase-matched DWs in the anomalous dispersion region, similar to bright solitons [40,41]. However, here, the value $\varepsilon = 0.0212$ is so small that the influence of HOD on the dark soliton and the energy emission can be ignored [37].

III. RESULT AND DISCUSSION

A. Mutual manipulation of soliton and probe wave

The nonlinear collision dynamics between a dark soliton in the normal dispersion regime and a probe wave in the anomalous dispersion regime can create an analog of the optical event horizon for special soliton grayness and probe wave parameters, which can provide possible methods for active manipulation of the interaction process. The wave number $D(\delta) = \delta^2/2 + \varepsilon\delta^3$ ($\delta = 2\pi f$; δ is the normalized angle frequency), and the relative group delay curve for a black soliton are shown in Fig. 1, which helps us to establish the main prerequisite for the optical event horizon, including both an effective refractive index barrier and copropagation of the two pulses with a near-identical group velocity. The two curves can be used as a reference for a gray soliton ($\phi = 0$), with just a slightly different group velocity resulting from the different phases. As shown in Fig. 1, when the frequencies of the probe wave lie in the light-green (yellow) -shaded area, the probe wave with a slower (faster) transmission speed will reflect on the leading (trailing) edge of the dark soliton, imitating group-velocity-led black (white) -hole horizon and produce an idle wave (reflected wave) with red (blue) -shift in frequency. It is worth noting that GVM is the transition point between the white- and black-hole horizons. Figure 2 summarizes the simulation results on the collision between a dark soliton with different grayness and a weak probe wave with varying intensities. Firstly, based on the phase-matching condition in Fig. 1, a weak probe wave, with the frequency offset −2.3 [Figs. 2(a1) and 2(c1)] or −2.7 [Figs. 2(b1) and 2(d1)], should temporally trail or precede with the dark soliton at the input to realize the collision in the regime of the optical event horizon in terms of their relative frequencies and the resulting different transmission velocities. A gray soliton traveling with a slightly different group velocity than that at the central carrier frequency (black soliton $\phi = 0$) acts as a moving refractive index barrier to prevent the low-power probe wave from passing through. Then the probe wave is elastically
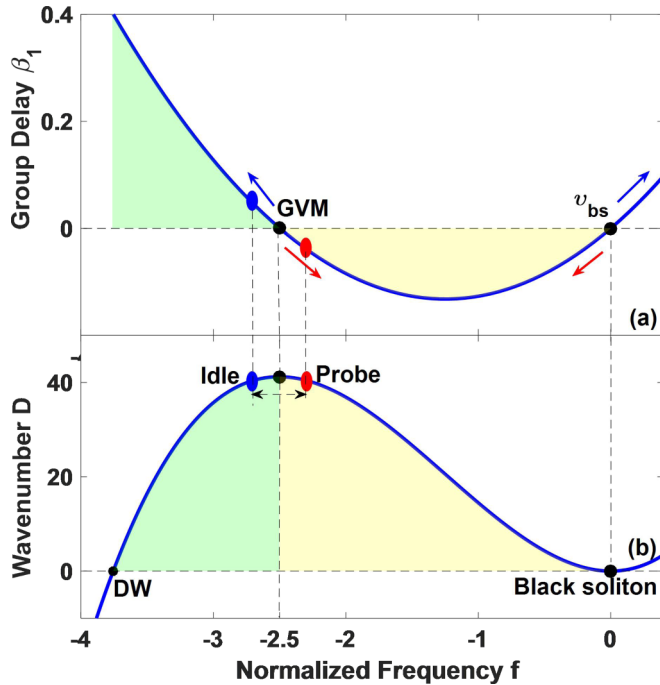
FIG. 1. The group delay curve (a) and the wave number (b) as a function of the normalized frequency for a black soliton. A phase-matched idler wave (reflected wave) is generated with opposite group velocity relative to the black soliton. v_{bs} is the group velocity of the black soliton and GVM is the corresponding group-velocity-matched point in frequency. DW is the phase-matched DW emitted by the black soliton. The blue arrows and the red arrows represent the changing trend of v_{bs} and the corresponding GVM point when the effective angle ϕ of the incident gray soliton is greater or less than zero, respectively.

scattered and partially transmitted. The dynamical process, relating to the analog of the white- or black-hole horizon, is shown in Figs. 2(a1) and 2(c1), and Figs. 2(b1) and 2(d1), respectively. In all cases, the dark soliton deviates from its original trajectory, being pushed by the weak but nonvanishing repulsive force from the probe wave. The change of the gray soliton group velocity is attributed to the change of soliton grayness after the collision, which manifests as a change in the color of gray solitons as shown in Figs. 3(a1)–3(d1). The probe wave benefiting from the typical "antiparticle" characteristic of a dark soliton is reflected on the optical event horizon during the collision. The deflection direction of the dark soliton trajectory is opposite to that of the probe wave, which is opposite to the case involving a bright soliton [23]. In addition, the grayness of the dark soliton in Figs. 2(a2) and 2(d2) increases, while that in Figs. 2(b2) and 2(c2) decreases. The change of grayness is determined by the intrinsic competition between the four-wave mixing (FWM) induced nonlinear phase shift of the dark soliton during the collision and the internal phase of the gray soliton. For the cases shown in Figs. 2(a2) and 2(d2), the nonlinear phase shift offsets a part of the internal phase when the probe wave collides with the dark soliton, so the grayness value of the gray soliton increases. Specifically, in the case for $\phi > 0$ in Figs. 2(a1) and 2(a2), the transmission velocity increases as well as the

time delay reduces. The evolution process is referred to as diametrically driven self-acceleration [42]. The case for $\phi < 0$ in Figs. 2(d1) and 2(d2) is opposite from the case of $\phi > 0$; its transmission speed decreases. While for the cases shown in Figs. 2(b2) and 2(c2), the nonlinear phase shift increases the internal phase of the gray soliton, so the soliton grayness decreases. The transmission velocity declines (raises) and the delay increases (reduces) in Fig. 2(b2) [Fig. 2(c2)]. In all cases, we see the dissipation effect of dark solitons, from the long oscillating tail with a stable amplitude and a similar period [37]. Subsequently, we adjust the intensity of the weak probe wave based on Figs. 2(a1)–2(d1) and the corresponding temporal output profiles of the dark soliton are plotted in Figs. 2(a3)–2(d3). On the one hand, when the peak power of the probe wave increases to $A_p = 0.31$ in Figs. 2(a3) and 2(d3), the nonlinear phase shift induced by the collision exactly cancels the internal phase of the gray soliton, transforming it into a black soliton. However, further increasing the probe wave power [$A_p = 0.4$ in Figs. 2(a3) and 2(d3)] induces a dominating nonlinear phase shift, converting the input gray soliton into another one with antiphase. On the other hand, the results in Figs. 2(b3) and 2(c3) demonstrate that increasing the intensity of the probe wave strengthens the internal phase of the gray soliton and results in the reduction of soliton grayness. So we can conclude that the interaction of the gray soliton with $\phi > 0$ ($\phi < 0$) with the leading (trailing) part of the probe wave can change them into dark solitons with smaller grayness, while interaction with the trailing (leading) part of the probe waves converts them into larger grayness ones. If the probe wave intensity is further increased, a black soliton and even another antiphase gray soliton can be acquired. In other words, when taking the group velocity at the center carrier frequency (the group velocity of the corresponding black soliton) as a reference, the collision induced by the movement between the dark soliton and the probe wave in the opposite direction increases the dark soliton grayness or even converts it into a "new" antiphase gray soliton, while the soliton grayness is reduced if the collision happens in the same direction. Furthermore, by comparing the results in Figs. 2(a) and 2(d), as well as Figs. 2(b) and 2(c), one can see clearly that the collision dynamics has some temporal-phase-frequency symmetry characteristics. These features are helpful to choose probe wave parameters according to different soliton properties to realize the soliton manipulation at the optical event horizon.

B. Impact of the dark soliton grayness on mutual manipulation

As shown in Figs. 2(a1) and 2(c1), as well as in Figs. 2(b1) and 2(d1), gray solitons with different phases exhibit distinct behaviors when interacting with the same probe wave in the regime of an optical event horizon. To analyze the relationship between this collision dynamics and the grayness value of the dark soliton, simulations with different ϕ are performed and the results are reported in Fig. 3 for the grayness value from $\phi = -\pi/3$ to $\phi = \pi/3$. All the other parameters in both Fig. 3(a) and the blue curve in Fig. 3(b) are the same as those in Fig. 2(a1). The white dashed line represents the position of the input probe wave. The energy conversion efficiency of the reflected wave decreases, while the frequency of the
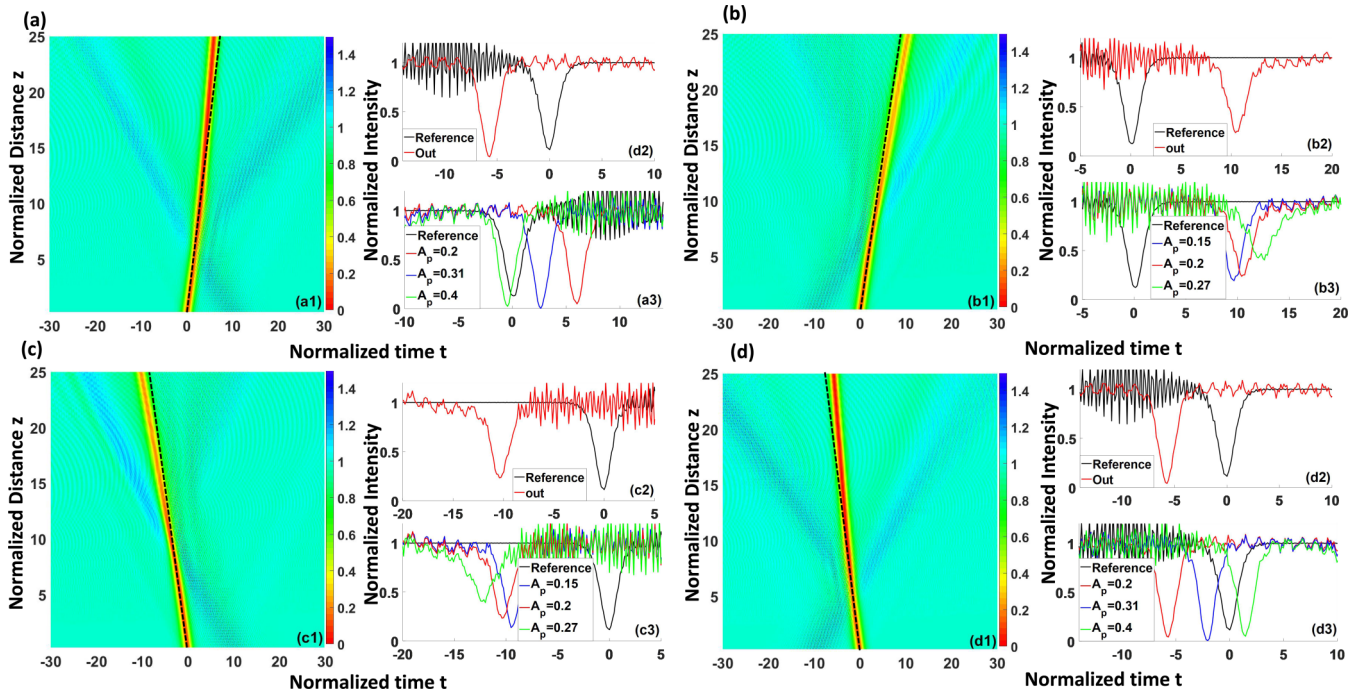
FIG. 2. Numerical simulations of the collision dynamics between a dark soliton with different grayness and a weak probe wave with varying intensities. (a) and (b) correspond to $\phi > 0$, while (c) and (d) correspond to $\phi < 0$. The frequency offset in (a) and (c) is -2.3, while it is -2.7 in (b) and (d). So the probe wave should temporally trail or precede the soliton to construct the optical event horizon. (a1)–(d1) plot the temporal evolutions as a function of the normalized transmission distance, and the corresponding input and output temporal profiles are shown in (a2)–(d2). (a3)–(d3) are the comparisons of input temporal profiles and the output temporal profiles for different input probe wave intensities. The black dashed lines in (a1)–(d1) are the original trajectories of the input dark soliton. The other parameters are all the same, as follows: $\phi = \pm\pi/10$, $T_1 = 3$, $t_1 = \pm10$.

reflected wave keeps widening toward the low-frequency region for the grayness value from $\phi = 0$ to $\phi = \pi/4$. That is because the input dark soliton with different grayness alters the corresponding phase-matching condition, resulting in the slower dark soliton and the frequency downshifting of both GVM and the newly generated reflected wave (blue arrow in Fig. 1), which is beneficial for the generation of supercontinuum without either soliton fission or modulation instability.
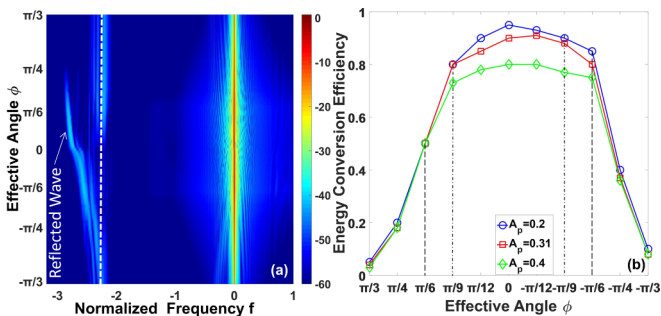

FIG. 3. The output spectrum profile (a) and the reflected wave energy conversion efficiency (b) versus the effective angle ϕ. The other parameters in both (a) and the blue curves in (b) are the same as those in Fig. 2(a1). The red and green curves in (b) correspond to an increased intensity of the probe wave to 0.31 and 0.4, respectively, and the white dashed line in (a) represents the input probe wave. The two black dashed lines and dash-dotted lines in (b) represent $\phi = \pm\pi/6$ and $\phi = \pm\pi/9$, respectively.

However, when the effective angle is larger than $\phi = \pi/4$, the group velocities of the two pulses are so different that there are not many overlapping interactions between them, and at the same time, the large phases ($|\phi|$) lead to the decrease in amplitude of the dark soliton and gradually tend to a flat continuous wave, both of these will make the energy conversion efficiency negligible. In that case, the probe wave is modulated by the dark soliton through FWM and presented as interference fringes in the frequency domain. Furthermore, when the effective angle evolves from $\phi = 0$ to $\phi = -\pi/4$, the frequency offset of the reflected wave decreases gradually due to the modified phase-matching condition (red arrow in Fig. 1, in which the GVM point keeps approaching the probe wave in frequency and the generated reflected wave moves to the high-frequency region). When the angle is smaller than $\phi = -\pi/4$, the group velocities of the two pulses are very similar and the reflected wave partially overlaps with the probe wave in the time domain, resulting in the temporal modulation of two pulses. What is more, the blue curve in Fig. 3(b) shows that the reflected wave energy conversion efficiency during the collision process presents a high value for the effective angle between $\phi = -\pi/6$ and $\phi = \pi/9$. When the effective angle tends to $\phi = \pi/3$ or $\phi = -\pi/3$, the reflected wave energy conversion efficiency decreases rapidly to a low value of less than 0.1. With the increase of the intensity of the probe wave, the energy conversion efficiency curves show the same trend but move down slightly as a whole. It is worth noting that the decreasing slope is much steeper
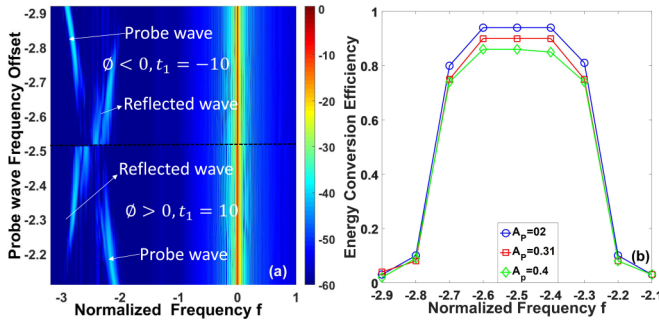
FIG. 4. The output spectrum (a) and the reflected wave energy conversion efficiency (b) versus the probe wave frequency offset. The probe wave with a normalized frequency less or greater than -2.5 initially precedes or trails the gray soliton temporally, corresponding to the dark soliton with $\phi < 0$ or $\phi > 0$. Here, the other parameters in both (a) and the blue curve in (b) are the same as those in Fig. 2(a1). The red and green curves in (b) show the results for increased intensity of the probe wave to 0.31 and 0.4, respectively. The upper and lower parts of the black dashed line in (a) are similar to the collision situation of Figs. 2(d1) and 2(a1), respectively.
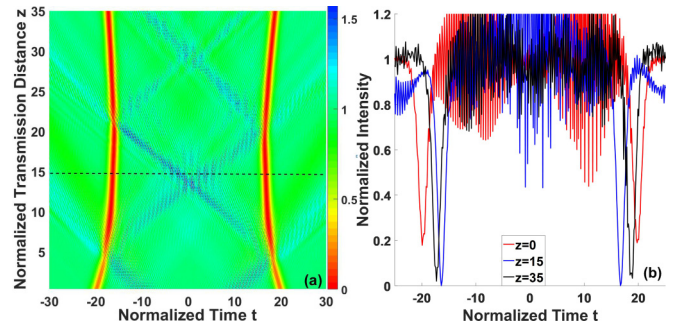

FIG. 5. (a) Density maps of the temporal evolution of the dark solitonic well as a function of transmission distance. (b) The temporal profile of the solitonic well at three representative transmission distances: $z = 0, 15, 35$. Here, $t_1 = 10$, $t_2 = 20$, $A_{p1} = 0.32$, $A_{p2} = 0.32$, $f_1 = -2.4$, and $f_1 = -2.6$; the other parameters are the same as those in Fig. 2(a1).

when the effective offset is between $f = -2.4$ and $f = -2.6$ and quickly decreases to almost zero at -2.9 and -2.1.

D. Formation and transformation of black-gray solitonic well

Based on the features obtained above during the evolution processes of collision dynamics, it is possible to generate a black-gray solitonic well in an optical fiber, where the white- and black-hole event horizons are combined. To demonstrate this, an initial electric field consisting of a pair of temporal-separated dark solitons and two temporal-frequent-separated probe waves is chosen:

$$
\begin{aligned}
A(0, t) = & A_{p1} \mathrm{sech}[(t + t_1)/T_1] \exp(-i2\pi f_1) \\
& + A_{p2} \mathrm{sech}[(t - t_1)/T_1] \exp(-i2\pi f_2) + A_{\mathrm{ds}2(0,t)},
\end{aligned}
\tag{5}
$$

with $A_{\mathrm{ds}2}$ taking the following form [18]:

$$
A_{\mathrm{ds}2}(0, t) = \begin{cases}
-u_0\{\cos\phi \tanh[u_0(t + t_2)\cos\phi] \\
\quad -i\sin\phi\}, & t < 0 \\
+u_0\{\cos\phi \tanh[u_0(t - t_2)\cos\phi] \\
\quad -i\sin\phi\}, & t \geqslant 0.
\end{cases}
\tag{6}
$$

Here, t_1 and t_2 stand for the pump position of the probe wave and the dark soliton, respectively. f_1 and f_2 represent the relative frequency offset of the two probe waves with respect to the central carrier frequency of the dark soliton. It should be noted that the grayness of the dark soliton, as well as the frequency of the probe wave, must be chosen reasonably according to the conclusions drawn earlier to ensure the effective transformation for the collision process. Here the grayness parameter of the dark soliton is $\phi = \pm\pi/10$ and the frequency offsets of the two probe waves are $f_1 = -2.4$ and $f_1 = -2.6$, respectively. Figure 5(a) shows the simulated temporal evolution of the four pulses copropagating along with the fiber, which can be divided into three regions. Before the first collision in the solitonic well, the two gray solitons with the same grayness value but opposite phase move toward each other with almost no perturbation due to no nonlinear interactions between the two pulses. Subsequently, they collide with the two probe waves at almost the same transmission distance;

C. Impact of the probe wave frequency on mutual manipulation

To better understand the collision dynamics in the regime of the optical event horizon, we studied the relationship between the probe wave frequency and the collision dynamics. As the situations show in Figs. 2(a) and 2(d), the gray soliton and the probe wave move toward each other, which plays a vital role in the active manipulation of the black-gray soliton transformation. The evolution of the fiber output spectrum and the reflected wave energy conversion efficiency as a function of the probe wave frequency offset are shown in Fig. 4. The GVM point of the corresponding black soliton is indicated by the dashed black line in Fig. 4(a). The probe wave with a normalized frequency less or greater than -2.5 initially precedes or trails the gray soliton temporally, corresponding to the soliton with $\phi < 0$ or $\phi > 0$. Then, these two waves collide. All the other parameters in both Fig. 4(a) and the blue curve in Fig. 4(b) are the same as those in Fig. 2. The spectrum evolutions in the range above -2.5 and below -2.5 are antisymmetric, which obey the phase-matching condition [in Fig. 1(b)] and are consistent with the results in Fig. 2. As shown in Fig. 4(a), when the frequency offset of the probe wave is above -2.2 or below -2.8, the probe wave and dark soliton penetrate each other due to the large group velocity difference, resulting in a very weak reflected wave. In addition, when the frequency offset of the probe wave is between -2.8 and -2.2, more energy is transferred from the probe wave to the reflected wave. For a frequency offset between -2.4 and -2.6, the probe wave is so close to the GVM point that the frequency offset of the reflected wave is small, and the weak probe wave and reflected wave are modulated, indicated by interference fringes in frequency. One can note that the reflected wave energy conversion efficiency is high

for an effective angle of less than 0. In Fig. 2, we can see that the collision dynamics have some time- symmetry, so the situation is just the opposite for the case of the probe wave leading.

then most of the probe wave energy is reflected by the gray soliton-induced refractive index barrier and trapped inside the solitonic well, with only a small part of the energy penetrating through. The temporal profile of the dark soliton at the normalized transmission distance of 15 in Fig. 5(b) shows that the pumped gray solitonic well is transformed into a black solitonic well after the collision. The leading and the trailing gray solitons shifting toward the outside of the solitonic well are converted into a faster and slower black soliton, respectively. Ultimately, the two newly generated black solitons colliding with the reflected waves turn into two gray solitons with opposite phase and larger grayness than the input two gray solitons. The temporal evolution process is due to the fact that the incident probe waves become the lower-energy reflection waves in the solitonic well after the first collision and then act as the probe waves during the next nonlinear collisions. This process realizes the transformation of the black-gray solitonic well. Although several similar evolutions are demonstrated in black and bright solitonic wells [20–22], here the gray solitonic well is mentioned. In Fig. 5, the gray solitonic well composed of two oppositely moving gray solitons increases the constraint distance of the solitonic well to the internal DWs, which is a significant feature of the solitonic well. Through the above discussion, the intrinsic manipulation mechanism is believed to be a wave blocking phenomenon that is also known from hydrodynamical systems.

IV. CONCLUSION

To conclude, we numerically demonstrate an approach of mutual manipulation between a dark soliton in the normal dispersion regime and a DW in the abnormal dispersion regime at the optical event horizon. Through the approach, we achieve both the trapping of DWs by the gray solitonic well and the transformation of gray and black solitonic wells. The gray-black soliton well proposed in our work increases the constraint distance of the solitonic well to the internal DWs, which is an important performance parameter of solitonic wells. In addition, the trapping efficiency of the soltion well is sensitive to both the grayness value of the input dark soliton and the frequency of the launched probe wave. The approach demonstrated in our work can be a qualified candidate for realizing the photonic transistorlike action and provides further insights into the collisional dynamics of dark solitons in a more controllable manner.

[1] K. Kondo, N. Ishikura, T. Tamura, and T. Baba, Temporal pulse compression by dynamic slow-light tuning in photonic-crystal waveguides, Phys. Rev. A **91**, 023831 (2015).

[2] S. Zhao, H. Yang, H. Huang, and Y. Xiao, Generation of tunable ultra-short pulse sequences in a quasi-discrete spectral supercontinuum by dark solitons, Opt. Express **27**, 23539 (2019).

[3] A. Demircan, S. Amiranashvili, C. Bree, C. Mahnke, F. Mitschke, and G. Steinmeyer, Rogue wave formation by accelerated solitons at an optical event horizon, Appl. Phys. B **115**, 343 (2014).

[4] A. Demircan, S. Amiranashvili, C. Bree, C. Mahnke, F. Mitschke, and G. Steinmeyer, Rogue events in the group velocity horizon, Sci. Rep. Lett. **2**, 850 (2012).

[5] D. Solli, C. Ropers, P. Koonath, and B. Jalali, Optical rogue waves, Nature (London) **450**, 1054 (2007).

[6] S. Robertson and U. Leonhardt, Frequency shifting at fiber-optical event horizons: The effect of Raman deceleration, Phys. Rev. A **81**, 063835 (2010).

[7] K. Webb, M. Erkintalo, Y. Xu, N. Broderick, J. Dudley, G. Genty, and S. Murdoch, Nonlinear optics of fibre event horizons, Nat. Commun. **5**, 4969 (2014).

[8] T. Philbin, C. Kuklewicz, S. Robertson, S. Hill, F. Konig, and U. Leonhardt, Fiber-optical analog of the event horizon, Science **319**, 1367 (2008).

[9] S. Hill, C. Kuklewicz, U. Leonhardt, and F. Konig, Evolution of light trapped by a soliton in a microstructured fiber, Opt. Express **17**, 13588 (2009).

[10] D. Faccio, S. Cacciatori, V. Gorini, V. Sala, A. Averchi, A. Lotti, M. Kolesik, and J. Moloney, Analogue gravity and ultrashort laser pulse filamentation, Europhys. Lett. **89**, 34004 (2010).

[11] A. Choudhary and F. Konig, Efficient frequency shifting of dispersive waves at solitons, Opt. Express **20**, 5538 (2012).

[12] S. F. Wang, A. Mussot, M. Conforti, A. Bendahmane, X. L. Zeng, and A. Kudlinski, Optical event horizons from the collision of a soliton and its own dispersive wave, Phys. Rev. A **92**, 023837 (2015).

[13] A. V. Yulin, R. Driben, B. A. Malomed, and D. V. Skryabin, Soliton interaction mediated by cascaded four wave mixing with dispersive waves, Opt. Express **21**, 14481 (2013).

[14] M. A. Gaafar, A. Y. Petrov, and M. Eich, Free carrier front induced indirect photonic transitions: A new paradigm for frequency manipulation on chip, ACS Photonics **4**, 2751 (2017).

[15] A. Efimov, A. V. Yulin, D. V. Skryabin, J. C. Knight, N. Joly, F. G. Omenetto, A. J. Taylor, and P. Russell, Interaction of an Optical Soliton with a Dispersive Wave, Phys. Rev. Lett. **95**, 213902 (2005).

[16] I. Oreshnikov, R. Driben, and A. V. Yulin, Interaction of high-order solitons with external dispersive waves, Opt. Lett. **40**, 5554 (2016).

[17] A. Demircan and Sh. Amiranashvili, Controlling Light by Light with an Optical Event Horizon, Phys. Rev. Lett. **106**, 163901 (2011).

[18] I. Oreshnikov, R. Driben, and A. V. Yulin, Weak and strong interactions between dark solitons and dispersive waves, Opt. Lett. **40**, 4871 (2015).

[19] Z. X. Deng, X. H. Shi, C. Tan, and X. Q. Fu, Reversible conversion between optical frequencies of probe and idler waves in regime of optical event horizon, J. Opt. Soc. Am. B **33**, 857 (2016).

[20] A. Demircan, S. Amiranashvili, C. Brée, and G. Steinmeyer, Compressible Octave Spanning Supercontinuum Generation by Two-Pulse Collisions, Phys. Rev. Lett. **110**, 233901 (2013).

[21] X. Liu, B. Zhou, H. Guo, and M. Bache, Mid-IR femtosecond frequency conversion by soliton-probe collision in phase-mismatched quadratic nonlinear crystals, Opt. Lett. **40**, 3798 (2015).

[22] Z. Deng, X. Fu, J. Liu, C. Zhao, and S. Wen, Trapping and controlling the dispersive wave within a solitonic well, Opt. Express **24**, 10302 (2016).

[23] S. F. Wang, A. Mussot, M. Conforti, X. L. Zeng, and A. Kudlinski, Bouncing of a dispersive wave in a solitonic cage, Opt. Lett. **40**, 3320 (2015).

[24] Z. X. Deng, J. Liu, X. W. Huang, C. J. Zhao, and X. L. Wang, Active control of adiabatic soliton fission by external dispersive wave at optical event horizon, Opt. Express **25**, 28556 (2017).

[25] C. Milián, T. Marest, A. Kudlinski, and D. V. Skryabin, Spectral wings of the fiber supercontinuum and the dark-bright soliton interaction, Opt. Express **25**, 10494 (2017).

[26] T. Marest, C. Masaraabi, M. Conforti, A. Mussot, C. Milian, D. V. Skryanin, and A. Kudlinski1, Collision between a dark soliton and a linear wave in an optical fiber, Opt. Express **18**, 23480 (2018).

[27] Z. Deng, Y. Chen, J. Liu, C. Zhao, and D. Fan, Optical event horizon-based complete transformation and control of dark solitons, Opt. Lett. **43**, 5327 (2018).

[28] Z. X. Deng, Y. Chen, J. Liu, C. Zhao, and D. Fan, Emission of multiple resonant radiations by spatiotemporal oscillation of multimode dark pulses, Opt. Express **27**, 36022 (2019)

[29] Y. S. Kivshar and B. Luther-Davies, Dark optical solitons: Physics and applications, Phys. Rep. **298**, 81 (1998).

[30] D. Krökel, N. J. Halas, G. Giuliani, and D. Grischkowsky, Dark-Pulse Propagation in Optical Fibers, Phys. Rev. Lett. **60**, 29 (1988).

[31] P. Emplit, J. P. Hamaide, F. Reynaud, C. Froehly, and A. Barthelemy, Picosecond steps and dark pulses through nonlinear single mode fibers, Opt. Commun. **62**, 374 (1987).

[32] A. Mahalingam and K. Porsezian, Propagation of dark solitons with higher-order effects in optical fibers, Phys. Rev. E **64**, 046608 (2001).

[33] C. Milián, D. V. Skryabin, and A. Ferrando, Continuum generation by dark solitons, Opt. Lett. **14**, 2096 (2009).

[34] T. Marest, C. Mas Arabí, M. Conforti, A. Mussot, C. Milián, D. V. Skryabin, and A. Kudlinski, Emission of dispersive waves from a train of dark solitons in optical fibers, Opt. Lett. **41**, 2454 (2016).

[35] T. Marest, C. Masarabi, M. Conforti, A. Mussot, C. Milian, D. V. Skryabin, and A. Kudlinski, Grayness-dependent emission of dispersive waves from dark solitons in optical fibers, Opt. Lett. **43**, 1511 (2018).

[36] Z. Deng, J. Liu, X. Huang, C. Zhao, and X. Wang, Dark solitons manipulation using optical event horizon, Opt. Express **26**, 16535 (2018).

[37] V. V. Afanasjev and Y. S. Kivshar, Effect of third-order dispersion on dark solitons, Opt. Lett. **24**, 1975 (1996).

[38] V. I. Karpman, Stationary and radiating dark solitons of the third order nonlinear Schrödinger equation, Phys. Lett. A **181**, 211 (1993).

[39] M. Selim Habib, C. Markos, O. Bang, and M. Bache, Soliton-plasma nonlinear dynamics in mid-IR gas-filled hollow-core fibers, Opt. Lett. **42**, 2232 (2017).

[40] J. Rong, H. Yang, and Y. Xiao, Accurately shaping supercontinuum spectrum via cascaded PCF, Sensors **20**, 2478 (2020).

[41] J. M. Dudley, G. Genty, and S. Coen, Supercontinuum generation in photonic crystal fiber, Rev. Mod. Phys. **78**, 1135 (2006).

[42] S. Batz and U. Peschel, Diametrically Driven Self-Accelerating Pulses in a Photonic Crystal Fiber, Phys. Rev. Lett. **110**, 193901 (2013).